reflection does not vary significantly along-axis[9], so we use a waveform inversion method that assumes that the layers are horizontally stratified. The inversion scheme is implemented in intercept time-slowness domain[23]. This transformation also allows a clear representation of the AMC and converted arrival ($P_{melt}S$) to be seen (Fig. 3) without interference of slow-phase-velocity events such as the sea-floor reflection. The waveform inversion method determines the P- and S-wave velocities of the crust by improving the fit between observed data and synthetically calculated data. It is an automated method, and therefore reduces human bias and also provides error estimates on the final solution[6,23]. The large-scale initial P-wave velocity was taken from Tolstoy *et al.*[9]. The initial S-wave velocity was obtained from the P-wave velocity assuming a Poisson's ratio of 0.26 (ref. 24). We used a P-wave attenuation coefficient of 16 for the first 200 m, and 40–90 for the crust below[24]. The S-wave attenuation coefficient was half of the P-wave attenuation coefficient. The model consists of a stack of 8-m-thick layers, for which the P-wave and S-wave velocities, density and attenuation are defined. This sampling interval was based on the minimum thickness that can be resolved from the observed data, which has a frequency bandwidth of 5–30 Hz. As data from all the slownesses were inverted simultaneously, the inverted results contain a model which is consistent with the data from all slownesses, and is therefore less likely to be influenced by incoherent noise due to two- and three-dimensional effects.

The turning rays above the sill and the P-wave reflection arrivals from the AMC constrain the P-wave and S-wave velocities above the AMC. Further constraint on S-wave velocity structure above the AMC comes from the arrival time of the $P_{melt}S$ phase. For this phase, the P-to-S conversion occurs at the solid–fluid interface of the AMC and at the sea bed such that the wave travels one leg between the sea bed and AMC as a P-wave, and the other as an S-wave. The waveforms of the AMC reflection and the $P_{melt}S$ phase constrain P-wave and S-wave velocities within the AMC and its neighbourhood. However, as with all seismic techniques, we have to guard against non-uniqueness of the final solution. To gain confidence in our results, we altered individual features within various candidate models while keeping the rest of the model fixed, and re-ran the inversion; the models that gave the best fit with the data are presented here.

Stacking. To enhance the partial-stack images, we firstly applied a frequency-wavenumber filter to the CMP gathers to remove sea-floor contamination of the AMC events, then performed a normal-moveout correction of 2.10 and 1.85 km s^{-1} for the P-wave and S-wave image, respectively. The partial stacks were obtained by stacking data between 2 and 3 km offsets, and all other processing parameters were as for the ~0–3 km offset stack. We note that the effect of two-dimensional scattering and multiple conversion points for $P_{melt}S$ will tend to provide a minimum estimate of the lateral extent of the pure melt zone. The absence of $P_{melt}S$ stack energy in the melt region could be due to the fact that the $P_{melt}S$ phase has two ray paths with slightly different points of conversion at the AMC that might affect the $P_{melt}S$ stack. Alternatively, the results could be confused by navigational error: that is, the ship track slipping off the axis in this region (Fig. 1).

Received 31 December 1997; accepted 28 May 1998.

1. Detrick, R. S. *et al.* Multi-channel seismic imaging of a crustal magma chamber along the East Pacific Rise. *Nature* **326,** 35–41 (1987).
2. Detrick, R. S. *et al.* Seismic structure of the southern East Pacific Rise. *Science* **259,** 499–503 (1993).
3. Kent, G. M., Harding, A. J. & Orcutt, J. A. Evidence for a smaller magma chamber beneath the East Pacific Rise at 9° 30′ N. *Nature* **344,** 650–653 (1990).
4. Mutter, J. C. *et al.* Magma distribution across ridge axis discontinuities on the East Pacific Rise from multi-channel seismic images. *Nature* **336,** 156–158 (1988).
5. Hussenoeder, S. A. *et al.* Seismic analysis of the axial magma chamber reflector along the southern East Pacific Rise from conventional reflection profiling. *J. Geophys. Res.* **101,** 22087–22105 (1996).
6. Collier, J. S. & Singh, S. C. Detailed structure of the top of the melt body beneath the East Pacific Rise at 9° 40′ N from waveform inversion of seismic reflection data. *J. Geophys. Res.* **102,** 20287–20304 (1997).
7. Kent, G. M., Harding, A. J. & Orcutt, J. A. Distribution of magma beneath the East Pacific Rise between the Clipperton transform and the 9° 17′ Deval from forward modelling of common depth point data. *J. Geophys. Res.* **98,** 13945–13970 (1993).
8. Kent, G. M., Harding, A. J. & Orcutt, J. A. Uniform accretion of oceanic crust south of the Garrett transform at 14° 15′ S on the East Pacific Rise. *J. Geophys. Res.* **99,** 9097–9116 (1994).
9. Tolstoy, M. *et al.* Deepening of the axial magma chamber on the southern East Pacific Rise towards the Garrett Fracture Zone. *J. Geophys. Res.* **102,** 3097–3108 (1997).
10. Schmeling, H. Numerical models on the influence of partial melt on elastic, anelastic and electrical properties of rocks: I Elasticity and anelasticity. *Phys. Earth. Planet. Inter.* **41,** 34–57 (1985).
11. Murase, T. & McBirney, A. R. Properties of some common igneous rocks and their melts at high temperature. *Geol. Soc. Am. Bull.* **84,** 3563–3592 (1973).
12. Manghnani, M. H., Sato, H. & Rai, C. S. Ultrasonic velocity and attenuation measurements on basalt melts to 1500 °C: Role of composition and structure in the visco-elastic properties. *J. Geophys. Res.* **91,** 9333–9342 (1986).
13. Mainprice, D. Modelling the anisotropic seismic properties of partially molten rocks found at mid-ocean ridges. *Tectonophysics* **279,** 161–179 (1997).
14. Marsh, B. D. Magma chamber. *Annu. Rev. Earth Planet. Sci.* **17,** 439–474 (1989).
15. Batiza, R. & Niu, Y. Petrology and magma chamber processes at the East Pacific Rise. *J. Geophys. Res.* **97,** 6779–6797 (1992).
16. Hooft, E. E., Detrick, R. S. & Kent, G. M. Seismic structure and indicators of magma budget along the southern East Pacific Rise. *J. Geophys. Res.* **102,** 27319–27340 (1997).
17. Collier, J. S. & Sinha, M. C. Seismic mapping of a magma chamber beneath the Valu Fa Ridge, Lau basin. *J. Geophys. Res.* **97,** 14031–14053 (1992).
18. Macdonald, K. C. *et al.* A new view of the mid-ocean ridge from the behaviour of ridge-axis discontinuities. *Nature* **335,** 217–225 (1988).
19. Sinton, J. M. *et al.* Magmatic process at superfast spreading mid-ocean ridges: Glass compositional variations along the East Pacific Rise 13°–23° S. *J. Geophys. Res.* **96,** 6133–6155 (1991).
20. Langmuir, C. H., Bender, J. F. & Batiza, R. Petrological and tectonic segmentation of the East Pacific Rise. *Nature* **322,** 422–429 (1986).
21. Worster, M. G., Huppert, H. E. & Sparks, R. S. Convection and crystallisation in magma cooled from above. *Earth Planet. Sci. Lett.* **101,** 79–89 (1990).
22. Scott, D. R. & Stevenson, D. J. A self-consistent model of melting, magma migration and buoyancy-driven circulation beneath mid-ocean ridges. *J. Geophys. Res.* **94,** 2973–2988 (1989).
23. Kormendi, F. & Dietrich, M. Non-linear waveform inversion of plane-wave seismograms in stratified elastic media. *Geophysics* **56,** 664–674 (1991).
24. Christeson, G. L., Wilcock, W. S. D. & Purdy, G. M. The shallow attenuation structure of the fast-spreading East Pacific Rise near 9° 30′ N. *Geophys. Res. Lett.* **21,** 321–324 (1994).
25. Tarantola, A. *Inverse Problem Theory* (Elsevier, New York, 1987).

Supplementary information is available on *Nature*'s World-Wide Web site (http://www.nature.com) or as paper copy from the London editorial office of *Nature*.

Acknowledgements. This work started when one of us (S.C.S.) was a Cecil Green Scholar at Scripps Institute of Oceanography. J.S.C. is supported by a NERC (BRIDGE) fellowship. Critical reviews from R. Detrick, M. Sinha and J. Garmany significantly improved this Letter.

Correspondence and requests for materials should be addressed to S.C.S. (e-mail: singh@esc.cam.ac.uk).

The intensity of the Earth's magnetic field over the past 160 million years

M. T. Juárez*, L. Tauxe†, J. S. Gee† & T. Pick‡

** Fort Hoofddijk Paleomagnetic Laboratory, Budapestlaan 17, 3584 CD Utrecht, The Netherlands*

† Scripps Institution of Oceanography, La Jolla, California 92093-0220, USA

‡ European Topic Center on Catalogue of Data Sources, Archivstrasse 2, D-30169 Hannover, Germany

In contrast to our detailed knowledge of the directional behaviour of the Earth's magnetic field during geological and historical times[1,2], data constraining the past intensity of the field remain relatively scarce. This is mainly due to the difficulty in obtaining reliable palaeointensity measurements, a problem that is intrinsic to the geological materials which record the Earth's magnetic field. Although the palaeointensity database has grown modestly over recent years[3–5], these data are restricted to a few geographical locations and more than one-third of the data record the field over only the past 5 Myr—the most recent database[5] covering the time interval from 5 to 160 Myr contains only about 100 palaeointensity measurements. Here we present 21 new data points from the interval 5–160 Myr obtained from submarine basalt glasses collected from locations throughout the world's oceans. Whereas previous estimates for the average dipole moment were comparable to that of the Earth's present field[6], the new data suggest an average dipole moment of $(4.2 \pm 2.3) \times 10^{22}$ A m^2, or approximately half the present magnetic-field intensity. This lower average value should provide an important constraint for future efforts to model the convective processes in the Earth's core which have been responsible for generating the magnetic field.

To augment the palaeointensity database, we focused on submarine basaltic glass (SBG) obtained from 20 sites sampled by the Deep Sea Drilling Project (DSDP). In addition to the DSDP glasses, we also include results from SBG obtained from pillow lavas in the Troodos ophiolite on Cyprus. SBG has been shown to contain predominantly single-domain magnetite as the carrier of the rema-

nent magnetization[7,8], based on a detailed rock-magnetic analysis. These studies also indicate that remanence-carrying grains alter little during heating in the laboratory. Analysis of SBG obtained from a recent lava flow recovered the geomagnetic field at the site[9]. These factors suggest that SBG is a nearly ideal material for palaeointensity studies.

The results presented here are from locations in both hemispheres, and are distributed throughout the world's oceans (Table 1). As the DSDP results were obtained from sites with identified marine magnetic anomalies, their ages are reasonably well constrained (Table 1). Moreover, tectonic-plate reconstructions allow adequate palaeolatitudes to be estimated and we therefore can calculate virtual axial dipole moments (VADMs) for samples spanning the past 160 Myr.

Our experimental design is based on the modified stepwise double heating method described in refs 10 and 11. Briefly, after measurement of the natural remanent magnetization (NRM), specimens are heated to a given temperature. They are then either cooled in zero field (to assess the decay of the NRM) or in an applied field (to assess the acquisition of partial-thermal remanent magnetization, p-TRM). After treatment at a given temperature step, an in-field step at a lower temperature can be repeated (a p-TRM check) to determine if the capacity to acquire thermal remanent magnetism (TRM) has remained constant or has changed because of chemical alteration of the samples at elevated temperatures.

As illustrated in Fig. 1, the behaviour of this new SBG sample collection is quite similar to that of SBG results described earlier[7–9], regardless of age or geographical location. Although DSDP glass samples are typically unorientated, we calculate the direction of the characteristic component and associated maximum angle of deviation[12] from the zero-field steps as a check on the validity of the palaeointensity results.

Maximum blocking temperatures of the NRM for most of the samples are generally between 475 and 550 °C, in agreement with previous results obtained for Cretaceous and Holocene SBG[7,8]. Regardless of the origin of remanence (whether a TRM or an early chemical remanence), the fact that SBG recovered from recent lava flows has similar rock magnetic characteristics and recovers the Earth's field accurately[9] lends support to our contention that SBG is a reliable recording medium of the Earth's palaeofield.

The wealth of data provided by the modified Thellier–Thellier technique as practised here allows ample information for objective data selection. Our criteria are as follows. (1) The component of magnetization used to determine palaeointensity must trend to the origin (within the maximum angle of deviation and the maximum angle of deviation must itself be $<15°$. (2) A best-fit line through the NRM/p-TRM data (see, for example, Fig. 1c and d) must have low scatter based on standard error of the slope (see, for example, ref. 11). (3) The p-TRM checks (triangles in Fig. 1c and d) must agree with the original p-TRM within 5%. (4) Data from multiple specimens of the same glassy margin must agree within 10%. These were then averaged to give a single palaeointensity estimate.

Data from specimens meeting the above criteria were deemed acceptable for palaeointensity calculations. Complete information concerning specimens used here is available: see Supplementary Information. Averages by hole are listed in Table 1.

The palaeointensity values from a single location are relatively uniform with the exception of those from Hole 238 (see Table 1) where two populations of intensity data can be statistically distinguished; the upper cores show higher values and are more scattered than the lower cores (Table 1). We have therefore split these data into two groups (upper and lower), and treat them as independent estimates of the geomagnetic field.

The absolute value of the slope of the best-fit line through the NRM/p-TRM data (see, for example, Fig. 1c and d) multiplied by the value of the magnetic field in the laboratory gives the absolute palaeofield (B) of the specimen in microteslas. These can be converted to VADMs, given the palaeolatitudes which were estimated using appropriate palaeomagnetic data[13–15] or plate reconstructions[16–18].

In Fig. 2 we plot VADM values for all samples of SBG available, including those previously published[7,9,19]. The VADM values for the

Table 1 Locations, ages, remanence and palaeointensity data for samples plotted in Fig. 2.

Hole*	Plate†	MMA‡	Age (Myr)§	λ/φ‖	λ′¶	B (s/n)#	VADM☆	M_n/M_{eq}**
504B	NZ	3A	6.4 ± 0.2	1/–84	1	30.3 ± 5.1 (3/3)	7.8 ± 1.3	6.6/6.6
395A	AF	4n	8 ± 1	23/–46	23	12.7 ± 8.2 (17/11)	2.6 ± 1.8	3.4/2.8
410/410A	NA	5n	10.3 ± 0.7	46/–30	45	10.8 ± 0.3 (4/3)	1.8 ± 0.1	3.2/2.0
396B	AF	5n	11.5 ± 0.5	23/–44	23	9.2 ± 2.2 (7/5)	2.0 ± 0.5	1.8/1.5
335	NA	5A-5B	13.8 ± 1.3	37/–35	37	16.2 ± 6.4 (10/9)	2.9 ± 1.1	3.7/2.6
520	AF	5Br	14.9 ± 0.2	–26/–11	–26	29.0 (2/1)	5.9	7.8/6.2
470A	NA	5B	15.7 ± 0.7	29/–118	24	31.7 ± 7.6 (3/3)	6.6 ± 1.6	5.3/4.3
562	NA	5Dr	17.9 ± 0.4	33/–42	32	13.6 ± 3.4 (9/9)	2.6 ± 0.6	3.3/2.4
495	CO	6	22 ± 2	12.5/–91	2	17.3 ± 2.1 (6/4)	4.4 ± 0.5	0.8/0.8
556	NA	12	32 ± 1.1	39/–35	36	15.8 ± 4.9 (5/4)	2.9 ± 0.9	3.3/2.3
559	NA	12r	32 ± 1.1	35/–41	32	9.5 ± 0.7 (3/2)	1.8 ± 0.1	0.5/0.4
563/564	NA	13	33.3 ± 0.3	34/–44	31	16.3 ± 3.2 (13/9)	3.1 ± 0.6	3.2/2.4
238 (upper)	IN	11 – 13	34 ± 4	–11/71	–24	33.0 ± 9.6 (5/3)	6.9 ± 2.0	1.7/1.4
238 (lower)	IN	11 – 13	34 ± 4	–11/71	–24	9.4 ± 0.5 (7/5)	2.0 ± 0.1	
407	NA	15r	35.2 ± 0.3	64/–31	60	27.9 ± 3.6 (5/4)	4.0 ± 0.5	5.0/2.8
522B	AF	16	35.7 ± 1.3	–27/–5	–30	19.6 ± 3.2 (6/4)	3.8 ± 0.6	5.0/3.8
447A	PH	18 – 21	43.5 ± 5.5	18/133	10	33.5 ± 0.7 (2/2)	8.3 ± 0.2	3.6/3.4
525A	AF	32n	72 ± 1	–29/3	–38	51.3 ± 3.9 (10/5)	9.0 ± 0.7	14.0/9.6
543A††	NA	34(y)	84	16/–60	–21	17.9 ± 2.2 (12/11)	2.0 ± 0.6	7.4/7.1
TR	AF	CNS	92	35/33	20	36.0 ± 6.9 (6/5)	7.9 ± 1.5	7.9/6.8
462A	NU	CNS	111 ± 1‖	7/165	–7	14.8 ± 0.4 (3/2)	3.7 ± 0.1	9.2/9.0
807C††	PA	CNS	122.3 ± 1	4/157	–34	19.4 ± 7.4 (30/18)	3.6 ± 1.4	5.9/4.2
417D††	NA	M0	125 ± 1	25/–68	17	12.0 ± 3 (12/11)	2.8 ± 0.7	9.2/8.2
418A††	NA	M0	125 ± 1	25/–68	17	15.5 ± 9 (12/11)	3.5 ± 1.9	13.6/12.1
534A	NA	M28	156.5 ± 0.1	28/–75	9	12.0 (1/1)	3.0	3.6/3.5

* DSDP/ODP hole, TR is Troodos ophiolite.
† Tectonic plate: AF, African; CO, Cocos; IN, Indian; NA, North American; NZ, Nazca; PH, Philippine; NU, Nauru.
‡ Marine magnetic anomaly (MMA) measured above site, CNS is the Cretaceous normal superchron.
§ Refs 33–36.
‖ Latitude (λ), and longitude (φ) of site in degrees.
¶ Estimated palaeolatitude in degrees (λ′, see text).
# Field intensity in μT (number of samples measured/number of samples used).
☆ Virtual axial dipole moment (10^{22} A m^2).
** NRM intensity and equatorial equivalent, in A m^{-1}. For sources, see Supplementary Information.
†† Data published earlier[9] and included for completeness.

pre-5-Myr data (Table 1) range from a minimum of 1.8×10^{22} A m^2 for Sites 410 and 559 (10 and 32 Myr, respectively) to a maximum of 9.0×10^{22} A m^2 for Site 525A (72 Myr). The average dipole moment calculated from these new data is $(4.2 \pm 2) \times 10^{22}$ A m^2, approximately half that of the present-day field. Furthermore, the highest values come from Late Cretaceous times (Hole 525A, and the Troodos ophiolite), a period with an anomalously low rate of reversals.

For comparison, we plot the palaeointensity database[5] as open circles in Fig. 2. Our only selection criteria for these data was that they be treated by a "Thellier" type of experiment, that they be "non-transitional" and that they have more than one specimen per site. There are 164 data points meeting these minimal criteria with ages between 0 and 160 Myr. In general, there is a fair degree of correspondence between the database and our new data set, although we find no high values in the time period around 15 Myr. Most of these high values come from the Steens Mountain study[20], a study with good temporal resolution. A single DSDP/ODP hole cannot hope to achieve the temporal resolution of such a stratigraphic profile, sampling instead at discrete intervals. It is therefore likely that the high values of the field evident in the Steens Mountain collection[20] were missed in our sample collection.

The remanent magnetization of the oceanic crust appears to undergo systematic variations over time[21]. We have compiled remanence values, M_{eq} (adjusted for the effects of palaeolatitude to equivalent equatorial values), for the dredge collections used in ref. 7, the Troodos pillow lavas, and DSDP basalts (Fig. 2). Data from DSDP/ODP holes were dated and adjusted for palaeolatitude in the same way as the palaeointensity data discussed above. The data that come from the same holes as our palaeointensity data are listed in Table 1. The complete data set is available: see Supplementary Information.

As illustrated in Fig. 2, ridge-crest basalts range in M_{eq} values

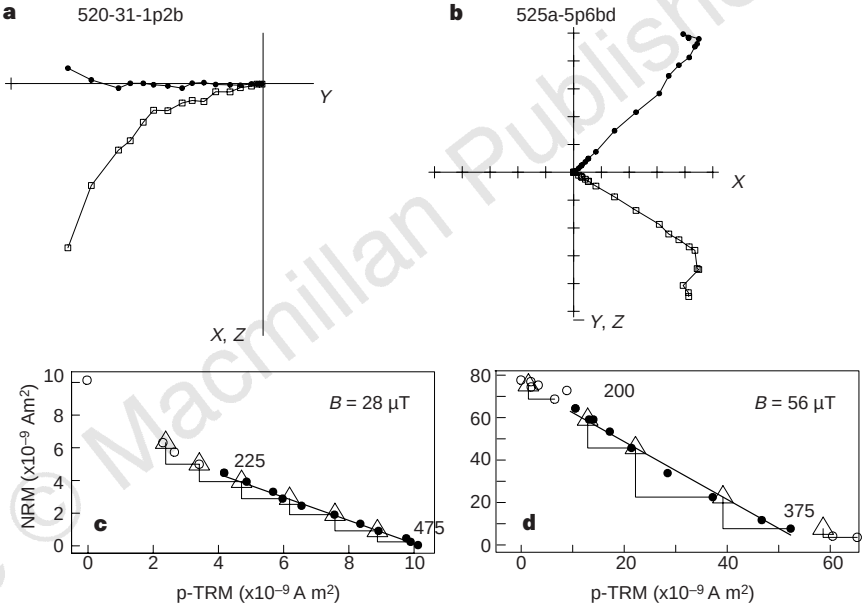

Figure 1 Behaviour of magnetic remanence during the Thellier–Thellier experiments. **a** and **b**, Vector end-point diagrams for the zero-field steps from 15-Myr and 72-Myr samples. Filled symbols are horizontal projections and open symbols are vertical projections. (Samples are unorientated). Treatment steps were: NRM, 100 °C, 150 °C then in 25 °C intervals to maximum. **c** and **d**, Plot of NRM remaining (zero-field steps) versus p-TRM gained (in field steps) from same samples shown in **a** and **b**. Filled symbols are used in the palaeofield calculation. Open triangles are the repeated p-TRM steps after heating to a higher temperature.

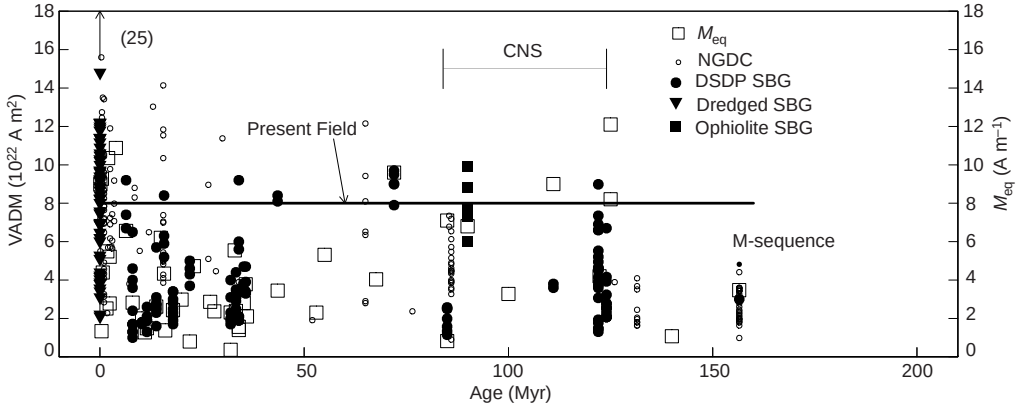

Figure 2 Summary of palaeointensity data for the past 160 Myr and NRM data from the DSDP/ODP basalts. Filled squares, estimated VADMs for palaeointensity from submarine basaltic glass (SBG); small circles, VADMs from the Thellier–Thellier database at the National Geophysical Data Center (NGDC); open squares, remanent magnetization (reduced to the equator, M_{eq}) of DSDP/ODP basalts versus age. Values of zero-age magnetization from ref. 32.

from less than 1 A m^{-1} to over 25 A m^{-1} at the ridge crest. With age, these values decrease rapidly to an average of several A m^{-1}. Values around 3 A m^{-1} are typical of DSDP basalts throughout the Neogene period. In the Late Cretaceous, high values of ~10 A m^{-1} are encountered, corresponding to the Cretaceous normal superchron (CNS) and a few million years after the end of the CNS. The period of time corresponding to the M-sequence anomalies (124–160 Myr) is characterized by low values of M_{eq} (and also by the "Mesozoic dipole low"[22]).

The general shape of the M_{eq} curve was first described by Bleil and Petersen[21]. The natural remanance of oceanic crustal rocks is controlled by a number of factors. Thermal remanence is controlled to first order by the intensity of the magnetic field and the amount and rock-magnetic characteristics of the magnetizable material in the rock. Even the youngest sea-floor basalts have apparently experienced some degree of alteration[23,24], and the exact behaviour of remanence during alteration is a complicated matter[25]. Thus, the long-term behaviour of the M_{eq} curve shown in Fig. 2 could result from (1) changes in palaeofield intensity, (2) changes in bulk chemistry (for example, Fe content), and/or (3) alteration history. Bleil and Petersen[21] argued that the behaviour of remanent intensities was primarily the result of gradual alteration of magnetic minerals of the oceanic crust by a mechanism of cation diffusion. Raymond and LaBrecque[26] proposed a quantitative alteration model in which a chemical remanent magnetization (CRM) is acquired as the original TRM is lost through low-temperature oxidation. According to their model, CRM acquired over the past 20 Myr could account for 80% of the variation in M_{eq}. Johnson and Pariso[27] argued that the cause of the observed variation of NRM in oceanic basalts was controlled primarily by differences in the original content of FeTi oxides in these older rocks. Thus, it would appear that the control of the long-term variation of the NRM of the ocean crust is still a matter of debate.

Although more difficult to demonstrate, some studies have suggested that a record of past geomagnetic intensity variations might be preserved in the magnetization of the ocean crust[28–30]. Several earlier investigations discounted the hypothesis that the intensity of the Earth's magnetic field played a significant role in the variations of the NRM on the basis of the lack of evidence for similar variations in the palaeointensity databases of the time. However, the new data set shown in Fig. 2 provides support for the view that the long-term variations in NRM of sea-floor basalts may, in large part, be a function of palaeofield intensity.

A last point that needs to be discussed concerns the effect that alteration of the magnetic minerals could have on the palaeointensity determinations. It is not yet completely clear whether our SBGs have undergone alteration that may have influenced their ability to record past geomagnetic intensity fluctuations. We deliberately select samples that have a 'fresh' appearance, excluding devitrified or evidently altered material. Although differentiating between TRM and CRM is still extremely difficult, the similarity in behaviour throughout our data set argues against gradual alteration. Because the youngest samples of SBG were collected within one year of eruption[9], any alteration that took place occurred within the first year, and produced a remanence that was indistingusihable from the original TRM.

Three conclusions can be drawn from our study. (1) Our data suggest that the average palaeofield intensity for the period 0–160 Myr is 4 ± 2 (10^{22} A m^2). These values are similar to the "Mesozoic dipole low" of Prévot *et al.*[22], suggesting that the Mesozoic field was not "low" but of average intensity. As has been previously suggested on the basis of analysis of marine magnetic anomalies[29], it appears that the present field may be anomalously high with respect to the long-term average dipole intensity. (2) In the collection of palaeointensity data from SBG, high palaeofield values are obtained for the most recent field[7] (the past 3 kyr) and for the Late Cretaceous (Table 1). The Late Cretaceous is characterized by a much lower rate of reversals than during the M-sequence or the Cenozoic era. The correspondence of higher field values with lower reversal rate is consistent with the data set of Tauxe and Hartl[31], who presented a correlation of relative palaeointensity data with polarity interval length. (3) To first order, the long-term trend in palaeointensity data from submarine basaltic glass parallels the trends in remanence behaviour from DSDP basals. This suggests that the remanence behaviour is controlled, at least in part, by geomagnetic field intensity variations. □

Received 2 March; accepted 3 June 1998.

1. Opdyke, N. D. & Channell, J. E. T. *Magnetic Stratigraphy* (Academic, San Diego, 1996).
2. Merrill, R. T., McElhinny, M. W. & McFadden, P. L. *Paleomagnetism, the Core, and the Deep Mantle* (Academic, San Diego, 1996).
3. McFadden, P. L. & McElhinny, M. W. Variations in the geomagnetic dipole 2: statistical analysis of VDM's for the past 5 m.y. *J. Geomagn. Geoelectr.* **34,** 163–189 (1982).
4. Tanaka, H., Kono, M. & Uchimura, H. Some global features of paleointensity in geological time. *Geophys. J. Int.* **120,** 97–102 (1995).
5. Perrin, M. & Shcherbakov, V. Paleointensity of the Earth's magnetic field for the past 400Ma: evidence for a dipole structure during the Mesozoic low. *J. Geomagn. Geoelectr.* **49,** 601–614 (1997); data available by anonymous ftp at ⟨ftp://ftp.ngdc.noaa.gov⟩ (cited 17 July 1998).
6. Merrill, R. T. & McElhinny, M. W. *The Earth's Magnetic Field* (Academic, San Diego, 1983).
7. Pick, T. & Tauxe, L. Holocene paleointensities: Thellier experiments on submarine basaltic glass from the East Pacific Rise. *J. Geophys. Res.* **98,** 17949–17964 (1993).
8. Pick, T. & Tauxe, L. Characteristics of magnetite in submarine basaltic glass. *Geophys. J. Int.* **119,** 116–128 (1994).
9. Pick, T. & Tauxe, L. Geomagnetic paleointensities during the Cretaceous normal superchron measured using submarine basaltic glass. *Nature* **366,** 129–139 (1993).
10. Thellier, E. & Thellier, O. Sur l'intensité du champ magnétique terrestre dans le passé historique et géologique. *Ann. Geophys.* **15,** 285–378 (1959).
11. Coe, R. S., Grommé, S. & Mankinen, E. A. Geomagnetic paleointensities from radiocarbon-dated lava flows on Hawaii and the question of the Pacific nondipole low. *J. Geophys. Res.* **83,** 1740–1756 (1978).
12. Kirschvink, J. L. The least-squares line and plane and the analysis of paleomagnetic data. *Geophys. J. R. Astron. Soc.* **62,** 699–718 (1980).
13. Van der Voo, R. *Paleomagnetism of the Atlantic, Tethys and Iapetus Oceans* (Cambridge Univ. Press, 1993).
14. Steiner, M. B. Paleomagnetism of the Cretaceous section, Site 462. *Init. Rep. DSDP* **61,** 711–716 (1981).
15. Clube, T. M. M., Creer, K. M. & Robertson, A. H. F. Paleorotation of the Troodos microplate, Cyprus. *Nature* **317,** 522–525 (1985).
16. Mueller, R. D., Royer, J.-Y. & Lawver, L. A. Revised plate motions relative to the hotspots from combined Atlantic and Indian Ocean hotspot tracks. *Geology* **21,** 275–278 (1993).
17. Lee, T.-Y. & Lawver, L. A. Cenozoic plate reconstruction of Southeast Asia. *Tectonophysics* **251,** 85–138 (1995).
18. Gripp, A. & Gordon, R. Plate velocities relative to hot spots. *Geophys. Res. Lett.* **17,** 1109–1112 (1990).
19. Mejia, V., Opdyke, N. D. & Perfit, M. R. Paleomagnetic field intensity recorded in submarine basaltic glass from the East Pacific Rise, the last 69 ka. *Geophys. Res. Lett.* **23,** 475–478 (1996).
20. Prévot, M., Mankinen, E. A., Coe, R. S. & Grommé, C. S. The Steens Mountain (Oregon) geomagnetic polarity transition 2. Field intensity variations and discussion of reversal models. *J. Geophys. Res.* **90,** 10417–10448 (1985).
21. Bleil, U. & Petersen, N. Variations in magnetization intensity and low-temperature titanomagnetite oxidation of ocean floor basalts. *Nature* **301,** 384–388 (1983).
22. Prévot, M., Derder, M. E. M., McWilliams, M. & Thompson, J. Intensity of the Earth's magnetic field: evidence for a Mesozoic dipole low. *Earth Planet. Sci. Lett.* **97,** 129–139 (1990).
23. Johnson, H. P. & Tivey, M. A. Magnetic properties of zero-age oceanic crust; a new submarine lava flow on the Juan de Fuca ridge. *Geophys. Res. Lett.* **22,** 175–178 (1995).
24. Kent, D. V. & Gee, J. Magnetic alteration of zero-age oceanic basalt. *Geology* **24,** 703–706 (1996).
25. Dunlop, D. J. & Özdemir, Ö. *Rock Magnetism: Fundamentals and Frontiers* (Cambridge Univ. Press, 1997).
26. Raymond, C. & LaBrecque, J. L. Magnetization of the oceanic crust: thermoremanent magnetization or chemical remanent magnetization? *J. Geophys. Res.* **92,** 8077–8088 (1987).
27. Johnson, H. P. & Pariso, J. E. Variations in oceanic crustal magnetization: Systematic changes in the last 160 million years. *J. Geophys. Res.* **98,** 435–445 (1994).
28. Cande S. C. & Kent, D. V. Ultrahigh resolution marine magnetic anomaly profiles: a record of continuous paleointensity variations? *J. Geophys. Res.* **97,** 15075–15083 (1992).
29. Gee, J., Schneider, D. A. & Kent, D. V. Marine magnetic anomalies as recorders of geomagnetic intensity variations. *Earth Planet. Sci. Lett.* **144,** 327–335 (1996).
30. Johnson, H. P., Vanpatten, D. & Sager, W. W. Age-dependent variation in the magnetization of seamounts. *Geophys. Res. Lett.* **22,** 231–234 (1995).
31. Tauxe, L. & Hartl, P. 11 million years of Oligocene geomagnetic field behaviour. *Geophys. J. Int.* **128,** 217–229 (1996).
32. Gee, J. & Kent, D. V. Magnetization of axial lavas from the southern East Pacific Rise (14 degrees–23 degrees S): Geochemical controls on magnetic properties. *J. Geophys. Res.* **10,** 24873–24886 (1997).
33. Castillo, P. R., Pringle, M. S. & Carlson, R. W. East Mariana Basin tholeiites: Cretaceous intraplate basalts or rift basalts related to the Ontong Java plume? *Earth Planet. Sci. Lett.* **123,** 139–154 (1994).
34. Mukasa & Ludden *Geology* **15,** 825 (1987).
35. Harland, W. B. *et al. A Geologic Time Scale* (Cambridge Univ. Press, 1989).
36. Cande, S. C. & Kent, D. V. Revised calibration of the geomagnetic polarity timescale for the Late Cretaceous and Cenozoic. *J. Geophys. Res.* **100,** 6093–6095 (1995).

Supplementary information is available on *Nature*'s World-Wide Web site (http://www.nature.com) or as paper copy from the London editorial office of *Nature*.

Acknowledgements. This work was supported in part by the NSF and GOA.

Correspondence and requests for materials should be addressed to L.T. (e-mail:ltauxe@ucsd.edu).